Matter and Radiation at Extremes | RESEARCH ARTICLE | scitation.org/journal/mre

Determination of laser entrance hole size for ignition-scale octahedral spherical hohlraums

Cite as: Matter Radiat. Extremes 7, 065901 (2022); doi: 10.1063/5.0102447
Submitted: 9 June 2022 • Accepted: 3 October 2022 •
Published Online: 26 October 2022

Yao-Hua Chen,[1] Zhichao Li,[2] Hui Cao,[1] Kaiqiang Pan,[2] Sanwei Li,[2] Xufei Xie,[2] Bo Deng,[2] Qiangqiang Wang,[2] Zhurong Cao,[2] Lifei Hou,[2] Xingsen Che,[2] Pin Yang,[2] Yingjie Li,[2] Xiaoan He,[2] Tao Xu,[2] Yonggang Liu,[2] Yulong Li,[2] Xiangming Liu,[2] Haijun Zhang,[2] Wei Zhang,[2] Baibin Jiang,[2] Jun Xie,[2] Wei Zhou,[2] Xiaoxia Huang,[2] Wen Yi Huo,[1] Guoli Ren,[1] Kai Li,[1] Xudeng Hang,[1] Shu Li,[1] Chuanlei Zhai,[1] Jie Liu,[3,4] Shiyang Zou,[1] Yongkun Ding,[1,4] and Ke Lan[1,4,a)]

AFFILIATIONS

[1] Institute of Applied Physics and Computational Mathematics, Beijing 100094, China
[2] Research Center of Laser Fusion, China Academy of Engineering Physics, Mianyang 621900, China
[3] Graduate School, China Academy of Engineering Physics, Beijing, China
[4] HEDPS, Center for Applied Physics and Technology, and College of Engineering, Peking University, Beijing 100871, China

[a)] **Author to whom correspondence should be addressed:** lan_ke@iapcm.ac.cn

ABSTRACT

A recently proposed octahedral spherical hohlraum with six laser entrance holes (LEHs) is an attractive concept for an upgraded laser facility aiming at a predictable and reproducible fusion gain with a simple target design. However, with the laser energies available at present, LEH size can be a critical issue. Owing to the uncertainties in simulation results, the LEH size should be determined on the basis of experimental evidence. However, determination of LEH size of an ignition target at a small-scale laser facility poses difficulties. In this paper, we propose to use the prepulse of an ignition pulse to determine the LEH size for ignition-scale hohlraums via LEH closure behavior, and we present convincing evidence from multiple diagnostics at the SGIII facility with ignition-scale hohlraum, laser prepulse, and laser beam size. The LEH closure observed in our experiment is in agreement with data from the National Ignition Facility. The total LEH area of the octahedral hohlraum is found to be very close to that of a cylindrical hohlraum, thus successfully demonstrating the feasibility of the octahedral hohlraum in terms of laser energy, which is crucially important for sizing an ignition-scale octahedrally configured laser system. This work provides a novel way to determine the LEH size of an ignition target at a small-scale laser facility, and it can be applied to other hohlraum configurations for the indirect drive approach.

I. INTRODUCTION

Achieving ignition is the major step on the path to controlled nuclear fusion energy, which has been a quest of scientists worldwide for more than a half a century.[1–3] Recently, the marvelous 1.37 MJ nuclear yield[4–7] of the National Ignition Facility (NIF)[8–10] is a clue that access to high fusion yields via indirect drive inertial confinement fusion may be attainable in the future. However, there are still major obstacles at the NIF to obtaining a predictable and reproducible fusion gain, such as irradiation asymmetry,[11–13] laser plasma instabilities (LPIs),[14–16] and hydrodynamic instabilities,[2,17,18] all of which are strongly connected with the hohlraum configuration and laser arrangement. The recently proposed octahedral spherical hohlraum[19–22] (hereinafter referred to simply as the octahedral hohlraum) with a single laser injection angle of 55° is an attractive concept for achieving a stable fusion gain at an upgraded facility[23] and can provide a high-symmetry drive on the capsule without any symmetry tuning. Experimental campaigns started in

2014 at the SG laser facility,[24] addressing the key issues regarding the design,[25–28] energetics,[29–31] and proof-of-concept[32] of the octahedral hohlraum. This novel approach has attracted broad interest in the fusion community.[33–39]

In contrast to cylindrical hohlraums with their two laser entrance holes (LEHs),[2,40–43] an octahedral hohlraum has six LEHs, and so LEH size can be a critical issue, given the laser energies that are available at present. As an example, we consider an Au octahedral hohlraum for the CH Rev5 ignition capsule[44] of the NIF, which can produce a clean one-dimensional (1D) yield 17.5 MJ according to Ref. 44. We calculate below the required laser energy and asymmetry of an octahedral hohlraum for this capsule. The absorbed laser energy E_{aL} of the hohlraum can be calculated using the energy balance[2,45,46]

$$\eta_{LX}E_{aL} = E_{\rm wall} + E_{\rm cap} + E_{\rm loss} = \sigma\tau T_r^4[(1-\alpha_W)A_W + (1-\alpha_C)A_C + A_{LEH}]. \quad (1)$$

Here, η_{LX} is the laser-to-x-ray conversion efficiency, $E_{\rm wall}$ and $E_{\rm cap}$ are the energies absorbed by the hohlraum wall and the capsule, and $E_{\rm loss}$ is the radiation loss via LEHs. σ is the Stefan–Boltzmann constant, τ is the effective laser pulse width, T_r is the radiation temperature, α_W is the wall albedo, α_C is the capsule albedo, A_W is the hohlraum wall area, A_C is the capsule surface area, and A_{LEH} is the total LEH area. From 2D simulations using the 2D multigroup radiation transfer hydrodynamic code LARED-Integration,[47,48] $\eta_{LX} \sim 87\%$ for an Au wall under an ignition pulse. From Ref. 44, we have a capsule diameter $\Phi_C = 2.216$ mm and $E_{\rm cap} = 165$ kJ, which gives $\alpha_C = 0.594$ under a 300 eV ignition pulse. We take the nominal laser energy from Ref. 44 as E_{aL} and the nominal peak laser power as the absorbed laser power P_{aL}. From $E_{aL} = 1.35$ MJ and $P_{aL} = 415$ TW, we have $\tau = 3.25$ ns. From the energy balance in Eq. (1), we find that for a 300 eV ignition pulse in the cylindrical hohlraum of Ref. 44 under such a laser, we have $\alpha_W = 0.91$. Taking η_{aL} as the laser absorption efficiency of the hohlraum, we obtain the required input laser energy as $E_L = E_{aL}/\eta_{aL}$. We take the unabsorbed light to be 10% for the octahedral hohlraum,[27] i.e., $\eta_{aL} = 90\%$. With these parameters, we can use the energy balance to calculate the required laser energy for the CH Rev5 capsule inside an octahedral hohlraum of diameter Φ_H with LEH diameter Φ_{LEH}. The result is E_L (MJ) $= 0.956 + 0.144[\Phi_{LEH}$ (mm)$]^2$ for $\Phi_H/\Phi_C = 4$, and E_L (MJ) $= 1.376 + 0.144[\Phi_{LEH}$ (mm)$]^2$ for $\Phi_H/\Phi_C = 5$.

To calculate the radiation asymmetry on the capsule, we expand the radiation flux on capsule surface as $\sum_{l=0}^{\infty}\sum_{m=-l}^{l} a_{lm}Y_{lm}(\theta,\phi)$, where $Y_{lm}(\theta,\phi)$ is the spherical harmonic of polar mode l and azimuthal mode m, and a_{lm} is the spherical harmonic decomposition. We define $C_{l0} = a_{l0}/a_{00}$ and $C_{lm} = a_{lm}/a_{00}$ for $m > 0$, and calculate C_{lm} with our 3D view factor code VF3D[20] by taking the relative fluxes of the laser spot, hohlraum wall, and LEH as 2:1:0.

In Tables I and II, we present C_{lm}, ϵ_{rms}, E_{aL}, E_L, and the radiation loss from LEHs for the CH Rev5 capsule inside octahedral hohlraums with $\Phi_H/\Phi_C = 4$ and 5, respectively, at $\Phi_{LEH} = 1.6$–3.6 mm. Here, ϵ_{rms} is the overall %rms including all modes.[3] We take the initial radii of the hohlraum and capsule in the calculation. It can be seen that Y_{2m} and Y_{lm} are absent for all odd l, because they are naturally zero in the octahedral geometry. For $\Phi_H/\Phi_C = 4$, Y_{40} dominates the asymmetry and increases with increasing Φ_{LEH}, with $Y_{40} < 1\%$ at $\Phi_{LEH} \le 3.6$ mm. For $\Phi_H/\Phi_C = 5$, termed the golden radius ratio in Ref. 20, the asymmetry is dominated by Y_{80}, with $Y_{80} < 3.4 \times 10^{-4}$ for all Φ_{LEH}. Thus, the asymmetry in all cases easily meets the ignition criterion of 1%.[2] However, E_{aL} is sensitive to Φ_{LEH}, because the six LEHs of larger size can lead to a remarkably high radiation energy loss. From Tables I and II, it can be seen that changing the LEH size makes a significant difference to the laser energy required. The calculations show that the energy requirement exceeds the present laser energy of 2 MJ at the NIF for $\Phi_{LEH} > 2.7$ mm at $\Phi_H = 8.864$ mm, and for $\Phi_{LEH} > 2.1$ mm at $\Phi_H = 11.08$ mm. Obviously, the upper limit of LEH size is restricted by the available laser energy. It seems that a smaller LEH should decrease E_{aL}; however, this is under the assumption that all laser beams can be fully injected into the hohlraum. If an LEH is small enough that some of the laser energy is blocked outside the hohlraum, greater laser energy will be needed to generate the required radiation temperature inside

TABLE I. C_{lm}, ϵ_{rms}, E_{aL}, E_L, and LEH loss of an octahedral hohlraum with $R_H = 4R_C$ for the CH Rev5 capsule, with Φ_{LEH} varying from 1.6 to 3.6 mm. Here, the LEH loss is the amount of input laser energy lost via the LEHs and is given by $E_{\rm loss}/\eta_{aL}\eta_{LX}$. In each case, the input laser energy E_L is chosen to give a radiation temperature of 300 eV.

Φ_{LEH} (mm)	1.6	2	2.4	2.8	3.2	3.6
C_{40}	1.7×10^{-3}	2.5×10^{-3}	3.4×10^{-3}	5.1×10^{-3}	7.1×10^{-3}	9.2×10^{-3}
C_{44}	1.0×10^{-3}	1.5×10^{-3}	2.1×10^{-3}	3.0×10^{-3}	4.2×10^{-3}	5.5×10^{-3}
C_{60}	1.6×10^{-6}	1.2×10^{-5}	2.8×10^{-5}	4.8×10^{-5}	6.7×10^{-5}	8.4×10^{-5}
C_{64}	1.7×10^{-6}	2.4×10^{-5}	5.3×10^{-5}	9.0×10^{-5}	1.2×10^{-4}	1.6×10^{-4}
C_{80}	8.6×10^{-4}	9.6×10^{-4}	1.0×10^{-3}	1.0×10^{-3}	8.1×10^{-4}	4.2×10^{-4}
C_{84}	3.2×10^{-4}	3.6×10^{-4}	3.9×10^{-4}	3.8×10^{-4}	3.1×10^{-4}	1.6×10^{-4}
C_{88}	4.9×10^{-4}	5.5×10^{-4}	5.9×10^{-4}	5.8×10^{-4}	4.6×10^{-4}	2.4×10^{-4}
ϵ_{rms}	2.6×10^{-3}	3.5×10^{-3}	4.7×10^{-3}	6.8×10^{-3}	9.3×10^{-3}	1.2×10^{-2}
E_{aL} (MJ)	1.19	1.38	1.61	1.88	2.19	2.54
E_L (MJ)	1.32	1.53	1.79	2.08	2.43	2.82
LEH loss (MJ)	0.40	0.63	0.91	1.24	1.62	2.05

TABLE II. C_{lm}, ϵ_{rms}, E_{aL}, E_L, and LEH loss of an octahedral hohlraum with $R_H = 5R_C$ for the CH Rev5 capsule, with Φ_{LEH} varying from 1.6 to 3.6 mm. The LEH loss is the same as in Table I, and is given here for comparison with E_L.

Φ_{LEH} (mm)	1.6	2	2.4	2.8	3.2	3.6
C_{40}	3.9×10^{-5}	5.6×10^{-5}	7.7×10^{-5}	1.0×10^{-4}	1.3×10^{-4}	1.8×10^{-4}
C_{44}	2.4×10^{-5}	3.4×10^{-5}	4.7×10^{-5}	6.1×10^{-5}	8.0×10^{-5}	1.1×10^{-4}
C_{60}	1.1×10^{-6}	1.5×10^{-5}	3.3×10^{-5}	5.1×10^{-5}	7.1×10^{-5}	9.7×10^{-5}
C_{64}	1.1×10^{-6}	2.9×10^{-5}	6.3×10^{-5}	9.7×10^{-5}	1.4×10^{-4}	1.8×10^{-4}
C_{80}	2.3×10^{-4}	2.7×10^{-4}	3.1×10^{-4}	3.3×10^{-4}	3.4×10^{-4}	3.2×10^{-4}
C_{84}	8.8×10^{-5}	1.0×10^{-4}	1.2×10^{-4}	1.2×10^{-4}	1.3×10^{-4}	1.2×10^{-4}
C_{88}	1.3×10^{-4}	1.6×10^{-4}	1.8×10^{-4}	1.9×10^{-4}	1.9×10^{-4}	1.8×10^{-4}
ϵ_{rms}	3.4×10^{-4}	3.9×10^{-4}	4.5×10^{-4}	5.3×10^{-4}	7.2×10^{-4}	6.0×10^{-4}
E_{aL} (MJ)	1.57	1.76	1.98	2.25	2.56	2.92
E_L (MJ)	1.74	1.95	2.21	2.50	2.85	3.24
LEH loss (MJ)	0.40	0.63	0.91	1.24	1.62	2.05

the hohlraum. Thus, the optimum LEH size should be a trade-off between clearance for the laser beams and available laser energy.

To have sufficient LEH clearance for the laser beams, the lower limit of LEH size is determined by three factors: (1) the focal spot size of the laser beam at the LEH, (2) the LEH closure caused by radiation, and (3) laser pointing error. Again considering the CH Rev5 capsule, the LEH closure under a 300 eV ignition pulse is about 0.29 mm according to our 1D multigroup radiation transfer hydrodynamic code RDMG.[49–51] Taking the pointing error as 0.08 mm for a laser beam of round shape with 1.2 mm diameter at the LEH, we estimate a LEH diameter $\Phi_{LEH} \sim 2$ mm.[21] Detail 2D simulations using LARED-Integration have shown that a value of $\Phi_{LEH} = 2.4$ mm can leave enough room[52] for this ignition target design. However, owing to the uncertainties in the simulation,[53] the LEH size should be determined with convincing experimental evidence before pursuing an ignition-scale laser system based on the octahedral hohlraum. Nevertheless, it remains a challenging task to determine the LEH size of an ignition target at a small-scale laser facility, because it is impossible to create ignition radiation inside an ignition-scale hohlraum with a small laser energy.

In this paper, we propose to use the prepulse of an ignition pulse to determine the LEH size of ignition-scale hohlraums via LEH closure behavior, and we present experimental evidence based on multiple diagnostics at the SGIII laser facility with the hohlraum, laser pre-pulse, and laser beam size at an ignition scale. As shown in Fig. 5 of Ref. 52, the LEH radius from simulations is a function of time under an ignition pulse, and it closes during the prepulse at low laser power but opens up again during the main pulse at high laser power. It is worth mentioning that this phenomenon has been clearly observed in NIF experiments.[54] Qualitatively, during the low-power part of the laser pulse, radiation-ablated plasma accumulates at the LEH and leads to a decrease in the open area of the LEH. On arrival of the main pulse, the ablated plasma is heated by the high-intensity laser, and the thermal pressure of the hot plasma pushes away the plasma entering the LEH, resulting in opening-up of the LEH.[52] This indicates that a given LEH size will be acceptable for the main pulse as long as it provides clearance for the laser beam during the prepulse. Thus, it should be possible to determine the appropriate LEH size for an ignition hohlraum by examining the LEH behavior during a prepulse generated at a small laser facility with an energy output lower than an ignition laser facility.

II. EXPERIMENTAL DESIGN

In the experiment, we consider an Au octahedral hohlraum of ignition-scale $\Phi_H = 8.8$ mm for a high-foot ignition scheme.[55] Note that LEH closure is caused mainly by radiation ablation if there is sufficient LEH clearance for the laser beams. In this case, a 2-LEH hohlraum has similar LEH closure behavior to a 6-LEH hohlraum under the same radiation drive. Hence, it is reasonable to use an ignition-scale hohlraum with two LEHs for this experiment. The hohlraum is initially filled with 1.3 mg/cm^3 C_5H_{12} gas at 0.4 atm pressure and room temperature. The required radiation temperature T_r and drive laser from LARED-Integration are presented in Fig. 1(a) for $\Phi_{LEH} = 2.2$ mm. As can be seen, the prepulse is composed of a picket, a first step, and a second step, with a laser power lower than 50 TW. The first and second steps start at 1.49 and 6 ns, respectively. The main pulse starts at 8.2 ns, rising rapidly to 500 TW within 0.8 ns. From postprocessing of 2D simulations, we can define various plasma interface positions for the LEH. As can be seen in Fig. 1(b), for all values of the electron density except for the very low $N_e = 0.1N_c$, the LEH radius keeps closing during the whole prepulse and then opens up after the main pulse starts, similar to what is shown in Fig. 5 of Ref. 52. Here, N_c is the laser critical density, $\sim 1.1 \times 10^{21}/\lambda^2$ cm^{-3}, where the laser wavelength λ is in micrometers. From 2D simulations, the beams have LEH clearance at $\Phi_{LEH} \geq 2.2$ mm, but they are severely blocked by LEH closure at $\Phi_{LEH} = 1.4$ mm.

The SGIII laser facility has an output of 180 kJ, an order of magnitude lower than the NIF, and is sufficiently flexible to create a ~10 ns laser pulse with power up to 50 TW. Hence, we can determine the LEH size by creating the prepulse inside an ignition-scale hohlraum with an ignition-scale laser beam size at SGIII. SGIII has 48 laser beams with injection angles of 28.5°, 35°, 49.5°, and 55°. Here, 55° happens to be the design angle of the octahedral hohlraum.[19–22] The laser pointing error is 0.07 mm. Figure 1(c) shows a schematic of the 2-LEH spherical hohlraum injected by the

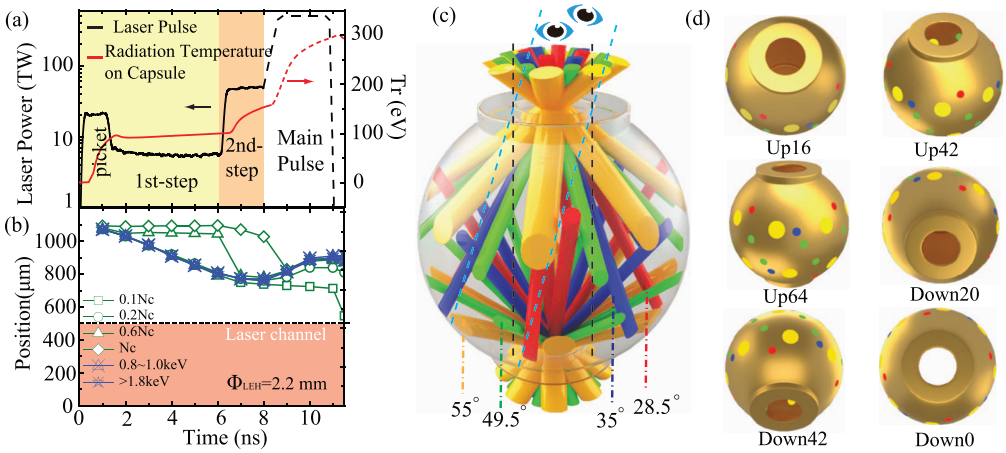

FIG. 1. (a) Required T_r (red curve) on the capsule of a high-foot scheme and the derived laser pulse (black curve) from 2D simulations for a 2-LEH spherical hohlraum with Φ_H = 8.8 mm and Φ_{LEH} = 2.2 mm. Only the prepulse (black solid curve) is considered in this experiment. (b) Post-processed time-dependent positions of plasma interface with electron density N_e = 0.1N_c, 0.2N_c, 0.6N_c, and N_c and positions of 50% peak x-ray emissions with energies between 0.8 and 1 keV or above 1.8 keV. The pink region is the laser channel. (c) Schematic of laser beam configuration and ignition-scale 2-LEH spherical hohlraum. The laser beams at 55° (orange) have a 1 mm diameter round shape at the LEH, and those at other angles have a 0.5 mm diameter. (d) Initial fields of view of the six flat-response x-ray detectors (FXRDs) and filtered M-band x-ray detectors (MXRDs), with the spots on the wall representing the laser depositions.

48 laser beams for this experiment. Every beam has a round shape at its LEH, with a super-Gaussian spatial profile $\propto \exp[-(2r/\Phi_Q)^m]$ produced using continuous phase plates (CPPs), with $m \sim 5$. Here, r is the spatial position along the radial direction of the LEH, and it includes 96% of the laser energy in the range $r \le \Phi_Q/2$. We use custom CPPs to have Φ_Q = 1 mm for the 16 beams at 55°, and the SGIII standard CPPs to have Φ_Q = 0.5 mm for the beams at other angles. We take Φ_Q as the beam size at the LEHs. According to our design, the 48 laser beams deliver about 110 kJ and 50 TW to create the prepulse in Fig. 1(a). In the experiment, to examine the LEH closure behavior at different LEH sizes, we take the LEH diameter as 1.4, 1.6, 1.8, 2, and 2.4 mm, respectively.

III. DIAGNOSTICS AND DISCUSSION

Various diagnostics[56] are used to provide experimental evidence to determine the LEH size. LEH closure is observed by an x-ray framing camera (XFC) through the upper LEH at 0° in two ranges of 0.8–1 keV (N-band emission of Au, mainly from the equilibrium region ablated by radiation) and 2–3 keV (M-band emission of Au, mainly from the nonequilibrium corona where most of the laser energy is absorbed). Time-integrated images of x-rays in 2–3 keV are also observed by a pinhole camera through the upper LEH at 16°. The x-ray emissions observed outside the LEH can provide important information on LEH closure. The x-ray fluxes of 0.1–5 keV are measured by an array of flat-response x-ray detectors (FXRDs) through the upper LEHs at 16°, 42°, and 64° and from the lower LEHs at 0°, 20°, and 42° with respect to the hohlraum axis. The M-band flux of x-rays >1.8 keV, largely emitted from the M-band of Au, is measured by an array of filtered M-band x-ray detectors (MXRDs) placed at the same places as the FXRDs. The measured fluxes vary with the viewing angles of the FXRDs and MXRDs, depending on the proportions of laser spot, re-emission wall, and LEH in their fields of view. The initial fields of view of all FXRDs and MXRDs are shown in Fig. 1(d) for Φ_{LEH} = 2.2 mm. The FXRDs and MXRDs at the upper 16° and 64° and the lower 64° positions can only see re-emissions from the wall. Laser spots can be viewed only by the FXRDs and MXRDs at the upper and lower 42° positions, with a proportion less than 10%. The on-axis FXRD and MXRD at 0° measure emissions from the plasmas accumulated around the hohlraum axis. Stimulated Brillouin and Raman backscattered lights are measured by a full-aperture backscatter station (FABS) and a near backscatter station (NBS) installed for beams at 55°. The total laser backscatter fraction is less than 4% for all shots, which is reasonable for such a prepulse with intensity less than 2.3×10^{14} W/cm^2.

On the left of Fig. 2, we present the time-resolved raw XFC images for shot SGIII20170323148 with Φ_{LEH} = 1.4 mm and shot SGIII20170324150 with Φ_{LEH} = 2 mm. The bright ring-shaped regions in these images are contributed by x-ray emissions from the ablated plasmas of the LEH edge. As can be seen, the LEH closure behaves similarly in the two x-ray bands for the same shot, but very differently between the two shots. The LEH with Φ_{LEH} = 1.4 mm closes before 6 ns and then opens up, while for Φ_{LEH} = 2 mm it continues to close at all times. This difference can be seen more clearly in the middle panels of Fig. 2, in which we present images along the temporal profiles of the drive laser together with the nominal radiation temperature T_r. Here, T_r is derived from the fluxes measured by the FXRDs,[31] varying with their fields of view. As can be seen, the LEH with Φ_{LEH} = 1.4 mm opens up after 6 ns when the second step pulse arrives with a rapid rise in power to about 50 TW. By contrast, the LEH with Φ_{LEH} = 2 mm continues to close throughout the pulse. From the XFC images, we can define the LEH radius as the central location of the sharp slope of the ring region,[54] and we show the time variation of this radius on the right of Fig. 2 for shots with Φ_{LEH} = 1.4 and 2 mm. It is obviously the high laser power of the sec-

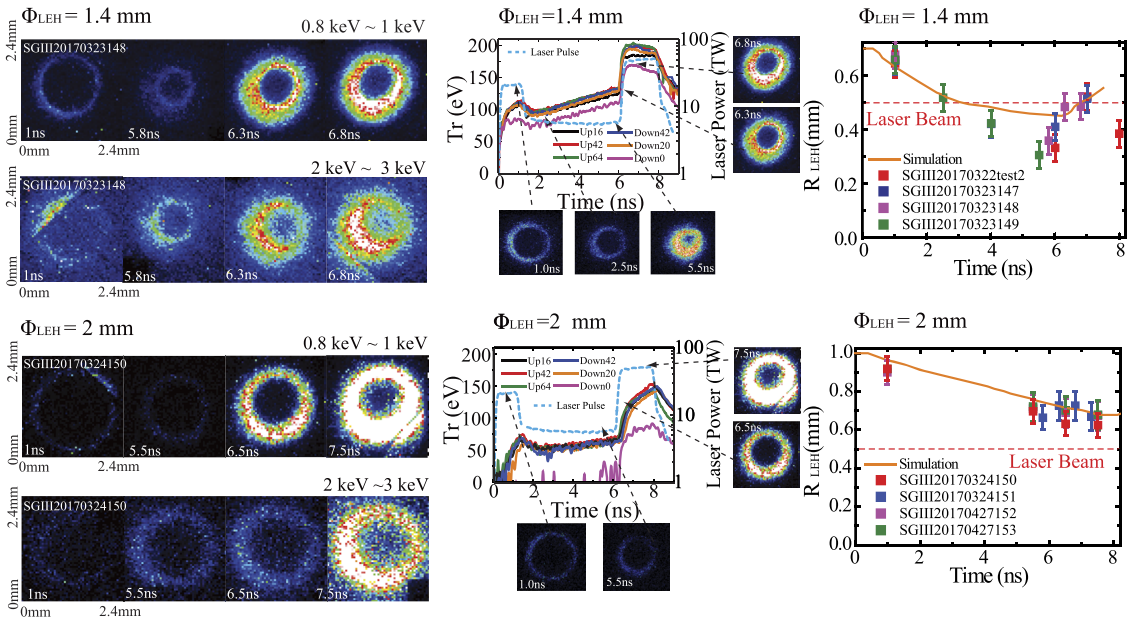

FIG. 2. (Left) Time-resolved raw images from an x-ray framing camera (XFC) at four different times and for two x-ray energy ranges of 0.8–1 and 2–3 keV for shot SGIII20170323148 with 1.4 mm diameter LEHs (upper) and shot SGIII20170324150 with 2 mm diameter LEHs (lower). (Middle) Drive laser power (light cyan dashed curve) and T_r (solid curves) with an error bar of 3% for shots SGIII20170323148 (upper) and SGIII20170324150 (lower). The small images match those on the left, except that the upper ones at 2.5 and 5.5 ns are for shot SGIII20170323149. (Right) Time-dependent LEH radius, defined as the half peak width of x-ray emissions of 0.8–1 keV, from XFC images (symbols with error bars of ±75 μm) and from post-shot 2D simulation (orange solid line) for shots with 1.4 mm diameter LEHs (upper) and 2 mm diameter LEHs (lower), with the red dashed line indicating the laser beam size. The mode 1 azimuthal asymmetry of the XFC images is due to the axis deviation between each pinhole and the XFC and to the axis deviation between the XFC and the target, which are considered in the error bars.

ond step that causes the transition from closure to opening up for Φ_{LEH} = 1.4 mm and slows down the closure for Φ_{LEH} = 2 mm. For comparison, we adopt this definition of the LEH radius in post-shot 2D simulations with LARED-Integration. The simulation results are also presented on the right of Fig. 2, from which it can be seen that they agree qualitatively with the observations.

Severe LEH closure for the case with Φ_{LEH} = 1.4 mm is confirmed by the interesting x-ray images from the pinhole camera for time-integrated M-band emissions of 2–3 keV. As can be seen in Fig. 3(a), the pinhole image of shot SGIII20170323149 has a strong emission ring (orange) from the inner edge of the LEH to the outer part of the laser channel, indicating strong M-band emission from the dense and hot plasmas that are ablated from the LEH edge and heated either directly by the lasers or by the hotter plasmas in the laser channel via electron heat conduction. Between the orange region and the LEH center, especially around the central part of the laser channel, M-band emissions become weak (light blue and blue) because of the relatively low density of the very hot laser plasmas in this region. The image in Fig. 3(a) clearly reveals that the radiation-ablated plasmas from the LEH edge strongly influence the

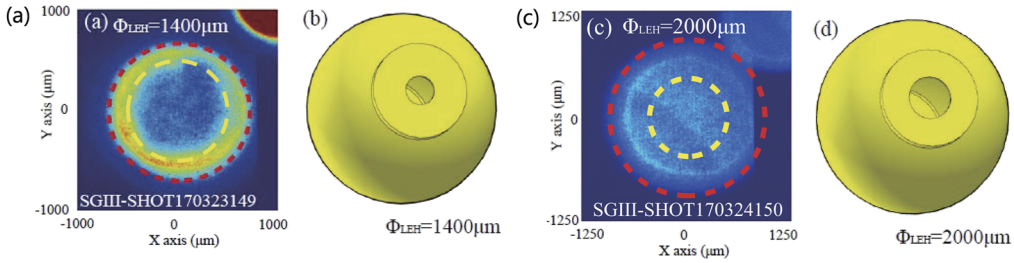

FIG. 3. (a) Time-integrated x-ray image at 2–3 keV observed by the pinhole camera at 16° from the upper side and (b) its field of view for shot SGIII20170323149 with 1.4 mm diameter LEHs. (c) and (d) Corresponding image and field of view for shot SGIII20170324150 with 2 mm diameter LEHs. The red dashed circle is the LEH edge and the yellow dashed circle is the outer boundary of the 1 mm diameter laser beam. Note that the size scales of the two images are different.

clearance of the laser channel for Φ_{LEH} = 1.4 mm. The time-integrated M-band emission images for Φ_{LEH} = 2 mm are quite different. As can be seen in Fig. 3(c), the time-integrated M-band emission is strong in a ring (light blue) between the LEH edge and the laser channel. The outer edge of this ring corresponds to the expanded LEH, which is too cold to emit many M-band x-rays, while the inner edge is at a low density and therefore is also unable to emit many M-band x-rays. The image in Fig. 3(c) clearly indicates that Φ_{LEH} = 2 mm provides sufficient clearance for the laser beams. Compared with the XFC image at 2–3 keV for shot SGIII20170324150 in Fig. 2, the time-integrated emission of this light blue ring is contributed mainly by the LEH closure plasmas at around 6.5 ns and later times. It is worth mentioning that the clear physical characteristics revealed by the images in Figs. 3(a) and 3(c) can be used to distinguish whether an LEH is open or not.

The severe LEH closure in the case of Φ_{LEH} = 1.4 mm is also confirmed by the temporal behavior of the M-band fluxes measured by the MXRDs. As can be seen in Fig. 4, the severe LEH closure for Φ_{LEH} = 1.4 mm leads to a strong M-band flux with very different temporal behavior from that for $\Phi_{LEH} \geq$ 1.8 mm. The M-band flux for Φ_{LEH} = 1.4 mm rises rapidly at 6 ns when the second step laser arrives, but rises much more slowly for $\Phi_{LEH} \geq$ 1.8 mm. In addition, the maximum M-band flux for Φ_{LEH} = 1.4 mm is about 18 times stronger than that for $\Phi_{LEH} \geq$ 1.8 mm. In particular, from the on-axis MXRD, it is found that the M-band flux is quite strong for Φ_{LEH} = 1.4 mm, while it is at a low noise level for $\Phi_{LEH} \geq$ 1.8 mm, except in the case Φ_{LEH} = 2.4 mm, which is somewhat abnormal. We have two shots for Φ_{LEH} = 1.6 mm. For shot SGIII20201009152, similar to Φ_{LEH} = 1.4 mm, the M-band flux from all MXRDs rises rapidly at 6 ns to a remarkably high maximum value. However, for shot SGIII20201010155, the M-band fluxes from all MXRDs behave similarly to those for $\Phi_{LEH} \geq$ 1.8 mm. This indicates that 1.6 mm may be a critical size for this model and that an LEH size $\Phi_{LEH} \geq$ 1.8 mm provides sufficient clearance for the laser beams. Thus, the measured M-band fluxes from MXRDs again provide strong evidence to determine the LEH size.

In Fig. 5, we compare the behavior of T_r for different values of Φ_{LEH}. As can be seen, for a given FXRD, T_r exhibits similar behavior for all shots with $\Phi_{LEH} \geq$ 1.8 mm, but there are remarkable differences in the case of Φ_{LEH} = 1.4 mm. First, for all FXRDs, for Φ_{LEH} = 1.4 mm, T_r rises more rapidly before the second step laser reaches its flat top and is much higher than that for $\Phi_{LEH} \geq$ 1.8 mm. Second, the T_r difference between on-axis and off-axis FXRDs for Φ_{LEH} = 1.4 mm is significantly smaller than for $\Phi_{LEH} \geq$ 1.8 mm. This indicates that the accumulated plasmas at the LEH lead to strong x-ray emission and severe LEH closure for Φ_{LEH} = 1.4 mm. Third, T_r for $\Phi_{LEH} \geq$ 1.8 mm continues to rise during the flat top of the second laser step and reaches a maximum when the laser ends, while T_r for Φ_{LEH} = 1.4 mm begins to decrease soon after the second step laser starts. This is a strong indication of severe LEH closure for Φ_{LEH} = 1.4 mm.

It should be noted here that T_r for Φ_{LEH} = 1.4 mm is much higher than for all other cases with larger Φ_{LEH}. Normally, a smaller Φ_{LEH} leads to a higher T_r inside the hohlraum because of lower radiation loss via the smaller LEH area. However, this is not the case for Φ_{LEH} = 1.4 mm, where the small size of the LEHs causes parts of the laser beams with Φ_Q = 1 mm to hit the LEH edge and the outer wall of the hohlraum, leading to strong x-ray emission out-

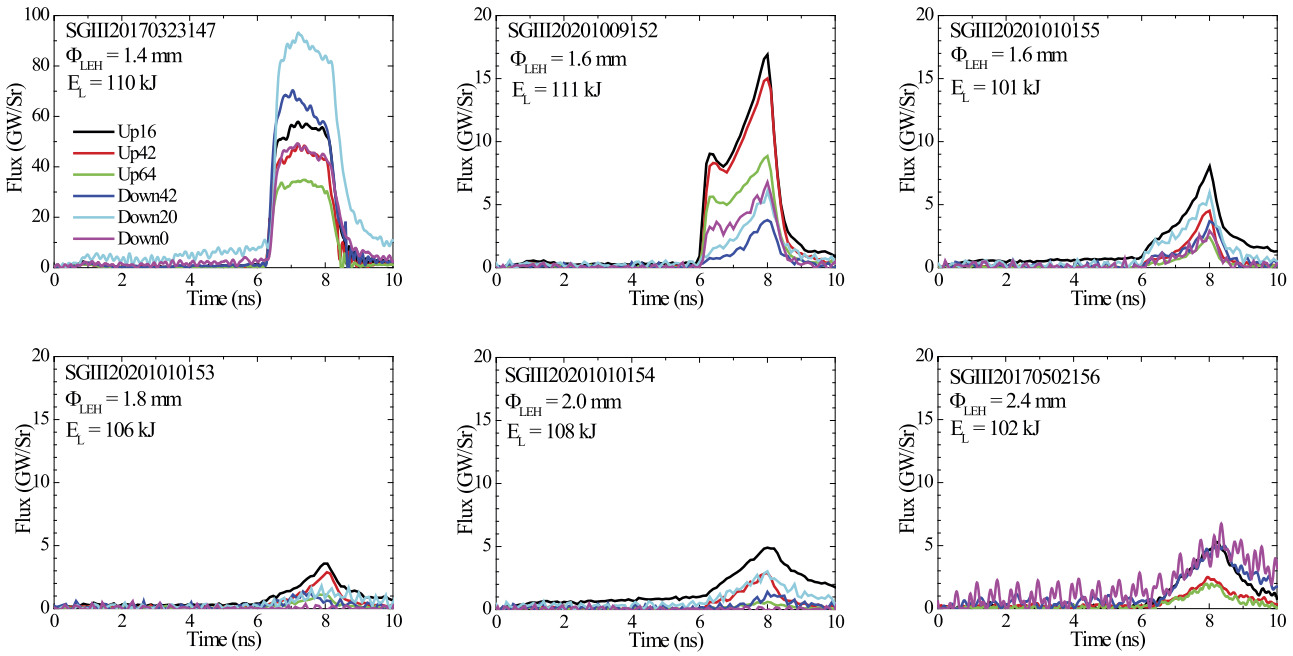

FIG. 4. Temporal behaviors of the M-band fluxes measured by the six MXRDs for shots with Φ_{LEH} = 1.4, 1.6, 1.8, 2, and 2.4 mm, with an error bar of 10%. The burrs on the curves are due to diagnostic noise at low fluxes. Note that the flux scale for Φ_{LEH} = 1.4 mm is different from the others.

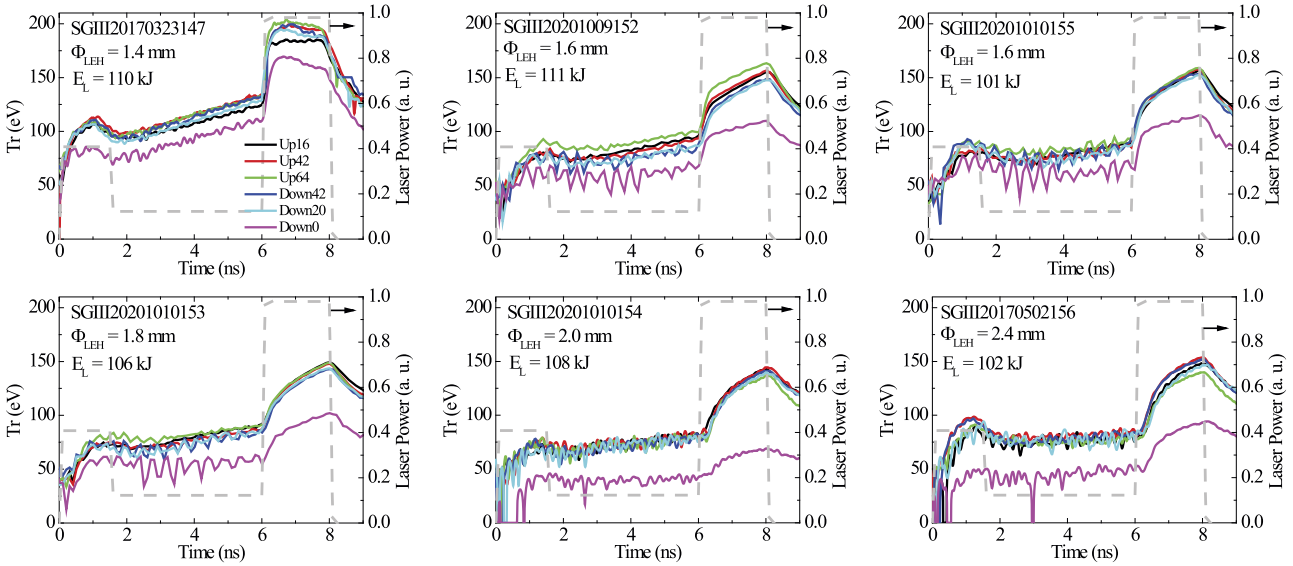

FIG. 5. Temporal behavior of T_r (solid curves) derived using the measured fluxes from six FXRDs for shots with Φ_{LEH} = 1.4, 1.6, 1.8, 2, and 2.4 mm. The laser power (light gray dashed lines) is shown for reference.

side the hohlraum. As a result, only part of the laser energy can be injected into the hohlraum, and a much lower T_r is generated inside the hohlraum than that measured by FXRDs outside the hohlraum. Thus, the much higher T_r for Φ_{LEH} = 1.4 mm from the FXRDs indicates a much lower T_r inside the hohlraum than in the cases with LEH clearance. It is interesting to note that the highest T_r of this "LEH closure" shot comes from the Up64 FXRD, which, although it sees a low flux (as shown in Fig. 4) because it views at a large angle to the hohlraum axis, also sees the hot LEH plasmas.

For an "LEH clearance" shot, the T_r values from all off-axis FXRDs are very close. This can be easily understood from their fields of view in Fig. 1(d), which are largely or even fully occupied by re-emissions from the wall. Note that from Fig. 5, the maximum T_r of the "LEH clearance" shots does not seem to be so sensitive to Φ_{LEH} once the differences of input laser energy are taken into account. In fact, from the energy balance, T_r increases about 3% from Φ_{LEH} = 1.4 to 2.4 mm inside such a 2-LEH spherical hohlraum with Φ_H = 8.8 mm, which is within the error bar of the FXRDs. We have two shots for Φ_{LEH} = 1.6 mm, whose T_r from off-axis FXRDs behave similarly to that for $\Phi_{LEH} \geq$ 1.8 mm, although the T_r from the on-axis FXRD rises rapidly at around 6 ns. Again, this indicates that Φ_{LEH} = 1.6 mm is a critical size for the model in this experiment. Considering the laser beam diameter of 1 mm at the LEHs and the laser pointing error of 0.07 mm, the LEH closure is less than 0.6 mm in diameter under the ignition prepulse used in this experiment, which is in agreement with NIF data. From the NIF, the measured LEH closure is about 0.515 mm in diameter according to Ref. 57 and 0.526 and 0.406 mm for the low-foot and high-foot schemes, respectively, according to Ref. 54. To leave enough room for the laser pointing accuracy, we determine that the LEH diameter should be 0.8 mm larger than the laser focal spot at the LEH.

IV. SUMMARY

We have proposed to use the prepulse of the ignition pulse to determine the LEH size for the ignition target via the LEH closure behavior at a small laser facility, and we have adopted this approach to determine the LEH size at the SGIII facility with convincing evidence from multiple diagnostics. As a result, we have found that it is safe to take an LEH 0.8 mm larger in diameter than the laser size at the LEH for the model in this experiment. Considering a laser with 1.2 mm diameter at the LEH, we can take Φ_{LEH} = 2 mm for an ignition octahedral hohlraum. This means that the octahedral hohlraum has the same total LEH area as that of an NIF cylindrical hohlraum.[13,58,59] The latter needs a larger LEH size for its inner beams, which are much larger than the outer beams[44,54] to suppress the serious LPIs arising from their long propagation distances inside the hohlraum. Taking Φ_{LEH} = 2 mm and assuming a laser backscatter of 10%, according to Tables I and II, 1.53 and 1.95 MJ are required to drive the 8.864 mm diameter and 11.08 mm diameter octahedral hohlraums, respectively,

Our work reported here has successfully demonstrated the feasibility of octahedral hohlraums for inertial confinement fusion and is crucially important for determining the appropriate dimensions for an octahedrally configured laser system to give a predictable and reproducible fusion gain.[23] It has also provided a novel way to determine the LEH size for an ignition-scale target at a small-scale laser facility. Note that the LEH closure is related to the prepulse. Hence, if a prepulse can ablate more plasmas and lead to more severe LEH closure, then a larger LEH will be required. Point designs with octahedral hohlraums for NIF capsules CH Rev5 and Be Rev6 are presented in Refs. 52 and 60 respectively, and a paper on point design for the recently proposed novel ignition capsule[61] is under preparation, which can mitigate the hydrodynamic instabilities by using CH

as the outermost ablator layer, while keeps high-density carbon as the main ablator for maintaining the advantage of short laser pulses.

ACKNOWLEDGMENTS

The authors thank the entire SGIII operations, diagnostics, and target teams at the Research Center of Laser Fusion, China Academy of Engineering Physics for their outstanding support during the experiment. All simulations were performed on a supercomputer in China. We especially acknowledge all the referees of this paper for providing very beneficial and important suggestions and questions to improve the quality of the paper. This work is supported by the National Natural Science Foundation of China (Grant No. 12035002).

AUTHOR DECLARATIONS

Conflict of Interest

The authors have no conflicts to disclose.

Author Contributions

Y.-H.C., Z.L., and Ke Lan contributed equally to this work. Y.-H.C. was lead scientist for the experiment in 2017 and performed simulations of pre- and post-shot studies for all shots in 2017. Z.L. was lead experimentalist on the experiment in 2017 and performed post-shot studies for all shots in 2017. H.C. was lead scientist for the experiment in 2020 and performed simulations of pre- and post-shot studies for all shots in 2020. K.P. was lead experimentalist on the experimental design in 2020 and performed post-shot studies for all shots in 2020. Sanwei Li, X.X., B.D., Q.W., Z.C., L.H., X.C., P.Y., Yingjie Li, Xiaoan He, T.X., Yonggang Liu, Yulong Li, and X.L. were responsible for diagnostics, building the experimental platform, and processing data. H.Z., Wei Zhang, and B.J. were responsible for target fabrication. Wei Zhou was responsible for laser operation. W.Y.H., G.R., Kai Li, Xudeng Hang, Shu Li, C.Z., J.L., S.Z., and Y.D. took part in discussions on the experiment. Ke Lan proposed the idea of using the prepulse of an ignition pulse to determine the LEH size of an ignition-scale hohlraum via LEH closure behavior, proposed the experimental design, and wrote the paper.

Yao-Hua Chen: Data curation (equal); Formal analysis (equal). **Zhichao Li**: Data curation (equal); Formal analysis (equal). **Hui Cao**: Formal analysis (supporting). **Kaiqiang Pan**: Data curation (supporting). **Sanwei Li**: Data curation (supporting). **Xufei Xie**: Data curation (supporting). **Bo Deng**: Data curation (supporting). **Qiangqiang Wang**: Data curation (supporting). **Zhurong Cao**: Data curation (supporting). **Lifei Hou**: Data curation (supporting). **Xingsen Che**: Data curation (supporting). **Pin Yang**: Data curation (supporting). **Yingjie Li**: Data curation (supporting). **Xiaoan He**: Data curation (supporting). **Tao Xu**: Data curation (supporting). **Yonggang Liu**: Data curation (supporting). **Yulong Li**: Data curation (supporting). **Xiangming Liu**: Data curation (supporting). **Haijun Zhang**: Data curation (supporting). **Wei Zhang**: Data curation (supporting). **Baibin Jiang**: Data curation (supporting). **Jun Xie**: Data curation (supporting). **Wei Zhou**: Data curation (supporting). **Xiaoxia Huang**: Data curation (supporting). **Wen Yi Huo**: Formal analysis (supporting). **Guoli Ren**: Formal analysis (supporting). **Kai Li**: Formal analysis (supporting). **Xudeng Hang**: Formal analysis (supporting). **Shu Li**: Formal analysis (supporting). **Chuanlei Zhai**: Formal analysis (supporting). **Jie Liu**: Formal analysis (supporting). **Shiyang Zou**: Formal analysis (supporting). **Yongkun Ding**: Formal analysis (supporting). **Ke Lan**: Conceptualization (equal); Data curation (equal); Formal analysis (equal).

DATA AVAILABILITY

The data that support the findings of this study are available within the article.

REFERENCES

[1] J. Nuckolls, L. Wood, A. Thiessen, and G. Zimmerman, "Laser compression of matter to super-high densities: Thermonuclear (CTR) applications," Nature **239**, 139 (1972).
[2] J. Lindl, "Development of the indirect-drive approach to inertial confinement fusion and the target physics basis for ignition and gain," Phys. Plasmas **2**, 3933 (1995).
[3] S. Atzeni and J. Meyer-ter-Vehn, *The Physics of Inertial Fusion* (Oxford Science, Oxford, 2004).
[4] D. Clery, "Laser-powered fusion effort nears 'ignition,'" Science **373**, 841 (2021).
[5] H. Abu-Shawareb, R. Acree, P. Adams, J. Adams, B. Addis, R. Aden *et al.*, "Lawson criterion for ignition exceeded in an inertial fusion experiment," Phys. Rev. Lett. **129**, 075001 (2022).
[6] A. B. Zylstra, A. L. Kritcher, O. A. Hurricane, D. A. Callahan, J. E. Ralph, D. T. Casey *et al.*, "Experimental achievement and signatures of ignition at the National Ignition Facility," Phys. Rev. E **106**, 025202 (2022).
[7] A. L. Kritcher, A. B. Zylstra, D. A. Callahan, O. A. Hurricane, C. R. Weber, D. S. Clark *et al.*, "Design of an inertial fusion experiment exceeding the Lawson criterion for ignition," Phys. Rev. E **106**, 025201 (2022).
[8] E. M. Campbell and W. J. Hogan, "The National Ignition Facility—Applications for inertial fusion energy and high-energy-density science," Plasma Phys. Controlled Fusion **41**, B39 (1999).
[9] C. A. Haynam, P. J. Wegner, J. M. Auerbach, M. W. Bowers, S. N. Dixit, G. V. Erbert *et al.*, "National Ignition Facility laser performance status," Appl. Opt. **46**, 3276 (2007).
[10] J. Nilsen, A. L. Kritcher, M. E. Martin, R. E. Tipton, H. D. Whitley, D. C. Swift *et al.*, "Understanding the effects of radiative preheat and self-emission from shock heating on equation of state measurement at 100s of Mbar using spherically converging shock waves in a NIF hohlraum," Matter Radiat. Extremes **5**, 018401 (2020).
[11] P. Michel *et al.*, "Tuning the implosion symmetry of ICF targets via controlled crossed-beam energy transfer," Phys. Rev. Lett. **102**, 025004 (2009).
[12] J. D. Moody, P. Michel, L. Divol, R. L. Berger, E. Bond, D. K. Bradley *et al.*, "Multistep redirection by cross-beam power transfer of ultrahigh-power lasers in a plasma," Nat. Phys. **8**, 344–349 (2012).
[13] A. B. Zylstra, O. A. Hurricane, D. A. Callahan, A. L. Kritcher, J. E. Ralph, H. F. Robey *et al.*, "Burning plasma achieved in inertial fusion," Nature **601**, 542 (2022).
[14] R. K. Kirkwood, J. D. Moody, J. Kline, E. Dewald, S. Glenzer, L. Divol *et al.*, "A review of laser-plasma interactions physics of indirect drive fusion plasma," Plasma Phys. Controlled Fusion **55**, 103001 (2013).
[15] E. L. Dewald, F. Hartemann, P. Michel, J. Milovich, M. Hohenberger, A. Pak *et al.*, "Generation and beaming of early hot electrons onto the capsule in laser-driven ignition hohlraums," Phys. Rev. Lett. **116**, 075003 (2016).
[16] V. T. Tikhonchuk, T. Gong, N. Jourdain, O. Renner, F. P. Condamine, K. Q. Pan *et al.*, "Studies of laser-plasma interaction physics with low-density targets for direct-drive inertial confinement fusion on the Shenguang III prototype," Matter Radiat. Extremes **6**, 025902 (2021).
[17] V. N. Goncharov, S. Skupsky, T. R. Boehly, J. P. Knauer, P. McKenty, V. A. Smalyuk *et al.*, "A model of laser imprinting," Phys. Plasmas **7**, 2062 (2000).
[18] A. Pak, L. Divol, C. R. Weber, L. F. B. Hopkins, D. S. Clark, E. L. Dewald *et al.*, "Impact of localized radiative loss on inertial confinement fusion implosions," Phys. Rev. Lett. **124**, 145001 (2020).

[19]K. Lan, J. Liu, D. Lai, W. Zheng, and X. He, "High flux symmetry of the spherical hohlraum with octahedral 6LEHs at a golden hohlraum-to-capsule radius ratio," arXiV:1311.1263v2 (2013).
[20]K. Lan, J. Liu, D. Lai, W. Zheng, and X.-T. He, "High flux symmetry of the spherical hohlraum with octahedral 6LEHs at the hohlraum-to-capsule radius ratio of 5.14," Phys. Plasmas **21**, 010704 (2014).
[21]K. Lan, X.-T. He, J. Liu, W. Zheng, and D. Lai, "Octahedral spherical hohlraum and its laser arrangement for inertial fusion," Phys. Plasmas **21**, 052704 (2014).
[22]K. Lan and W. Zheng, "Novel spherical hohlraum with cylindrical laser entrance holes and shields," Phys. Plasmas **21**, 090704 (2014).
[23]K. Lan, "Dream fusion in octahedral spherical hohlraum," Matter Radiat. Extremes **7**, 055701 (2022).
[24]K. Lan, J. Liu, Z. Li, X. Xie, W. Huo, Y. Chen *et al.*, "Progress in octahedral spherical hohlraum study," Matter Radiat. Extremes **1**, 8 (2016).
[25]W. Huo, Z. Li, D. Yang, K. Lan, J. Liu, G. Ren *et al.*, "First demonstration of improving laser propagation inside the spherical hohlraums by using the cylindrical laser entrance hole," Matter Radiat. Extremes **1**, 2 (2016).
[26]Z. Li, D. Yang, S. Li, W. Y. Huo, K. Lan, J. Liu, G. Ren *et al.*, "Comparison of the laser spot movement inside cylindrical and spherical hohlraums," Phys. Plasmas **24**, 072711 (2017).
[27]K. Lan, Z. Li, X. Xie, Y. H. Chen, C. Zheng, C. Zhai *et al.*, "Experimental demonstration of low laser-plasma instabilities in gas-filled spherical hohlraums at laser injection angle designed for ignition target," Phys. Rev. E **95**, 031202(R) (2017).
[28]Y. Chen, Z. Li, X. Xie, C. Zheng, C. Zhai, L. Hao *et al.*, "First experimental comparisons of laser-plasma interactions between spherical and cylindrical hohlraums at SGIII laser facility," Matter Radiat. Extremes **2**, 77 (2017).
[29]W. Y. Huo, Z. Li, Y. H. Chen, X. Xie, K. Lan, J. Liu *et al.*, "First investigation on the radiation field of the spherical hohlraum," Phys. Rev. Lett. **117**, 025002 (2016).
[30]X. Xie, Z. Li, S. Li, Y. Huang, L. Jing, D. Yang *et al.*, "Radiation flux study of spherical hohlraums at the SGIII prototype facility," Phys. Plasmas **23**, 112701 (2016).
[31]W. Y. Huo, Z. Li, Y.-H. Chen, X. Xie, G. Ren, H. Cao *et al.*, "First octahedral spherical hohlraum energetics experiment at the SGIII laser facility," Phys. Rev. Lett. **120**, 165001 (2018).
[32]K. Lan, Y. Dong, J. Wu, Z. Li, Y. Chen, H. Cao *et al.*, "First inertial confinement fusion implosion experiment in octahedral spherical hohlraum," Phys. Rev. Lett. **127**, 245001 (2021).
[33]L. Ren, D. Zhao, and J. Zhu, "Beam guiding system geometric arrangement in the target area of high-power laser drivers," High Power Laser Sci. Eng. **3**, e12 (2015).
[34]P. E. Masson-Laborde, M. C. Monteil, V. Tassin, F. Philippe, P. Gauthier, A. Casner *et al.*, "Laser plasma interaction on rugby hohlraum on the Omega Laser Facility: Comparisons between cylinder, rugby, and elliptical hohlraums," Phys. Plasmas **23**, 022703 (2016).
[35]W. A. Farmer, M. Tabak, J. H. Hammer, P. A. Amendt, and D. E. Hinkel, "High-temperature hohlraum designs with multiple laser-entrance holes," Phys. Plasmas **26**, 032701 (2019).
[36]W. Wang and R. S. Craxton, "Development of a beam configuration for the SG4 laser to support both direct and indirect drive," https://www.lle.rochester.edu/media/publications/high_school_reports/documents/hs_reports/2019/Wang_William.pdf, August 2020.
[37]S. Craxton, "A new beam configuration to support both spherical hohlraums and symmetric direct drive," in The 62nd Annual Meeting of the American Physical Society Division of Plasma Physics, USA, November 9–13, 2020.
[38]W. Y. Wang and R. S. Craxton, "Pentagonal prism spherical hohlraums for OMEGA," Phys. Plasmas **28**, 062703 (2021).
[39]W. Y. Wang and R. S. Craxton, "A proposal for pentagonal prism spherical hohlraum experiments on OMEGA," https://www.lle.rochester.edu/media/publications/lle_review/documents/v166/166_02_Wang.pdf, Jan-Mar 2021.
[40]M. Vandenboomgaerde, J. Bastian, A. Casner, D. Galmiche, J. P. Jadaud, S. Laffite *et al.*, "Prolate-spheroid ("rugby-shaped") hohlraum for inertial confinement fusion," Phys. Rev. Lett. **99**, 065004 (2007).
[41]K. Lan, D. Lai, Y. Zhao, and X. Li, "Initial study and design on ignition ellipraum," Laser Part. Beams **30**, 175 (2012).
[42]S. Le Pape, L. F. Berzak Hopkins, L. Divol, A. Pak, E. L. Dewald, S. Bhandarkar *et al.*, "Fusion energy output greater than the kinetic energy of an imploding shell at the National Ignition Facility," Phys. Rev. Lett. **120**, 245003 (2018).
[43]P. Amendt, D. Ho, Y. Ping, V. Smalyuk, S. Khan, J. Lindl *et al.*, "Ultra-high (>30%) coupling efficiency designs for demonstrating central hot-spot ignition on the National Ignition Facility using a Frustraum," Phys. Plasmas **26**, 082707 (2019).
[44]S. W. Haan, J. D. Lindl, D. A. Callahan, D. S. Clark, J. D. Salmonson, B. A. Hammel *et al.*, "Point design targets, specifications, and requirements for the 2010 ignition campaign on the National Ignition Facility," Phys. Plasmas **18**, 051001 (2011).
[45]K. Lan, P. Gu, G. Ren, X. Li, C. Wu, W. Huo, D. Lai, and X.-T. He, "An initial design of hohlraum driven by a shaped laser pulse," Laser Part. Beams **28**, 421 (2010).
[46]R. Sigel, R. Pakula, S. Sakabe, and G. D. Tsakiris, "X-ray generation in a cavity heated by 1.3 or 0.44 mm laser light III Comparison of the experimental results with theoretical predictions for x-ray confinement," Phys. Rev. A **38**, 5779–5785 (1988).
[47]K. Lan, T. Feng, D. Lai, Y. Xu, and X. Meng, "Study on two-dimensional transfer of radiative heating wave," Laser Part. Beams **23**, 275 (2005).
[48]H. Yong, P. Song, C.-L. Zhai, D.-G. Kang, J.-F. Gu, X.-D. Hang, P.-J. Gu, and S. Jiang, "Numerical simulation of 2-D radiation-drive ignition implosion process," Commun. Theor. Phys. **59**, 737 (2013).
[49]Y. Li, K. Lan, D. Lai, Y. Gao, and W. Pei, "Radiation-temperature shock scaling of 1 ns laser-driven hohlraums," Phys. Plasmas **17**, 042704 (2010).
[50]W. Y. Huo, K. Lan, Y. Li, D. Yang, S. Li, X. Li *et al.*, "Determination of the hohlraum M-band fraction by a shock-wave technique on the SGIII-prototype laser facility," Phys. Rev. Lett. **109**, 145004 (2012).
[51]X. Qiao and K. Lan, "Study of high-Z-coated ignition target by detailed configuration accounting atomic physics for direct-drive inertial confinement fusion," Plasma Phys. Controlled Fusion **61**, 014006 (2019).
[52]H. Cao, Y.-H. Chen, C. Zhai, C. Zheng, and K. Lan, "Design of octahedral spherical hohlraum for CH Rev5 ignition capsule," Phys. Plasmas **24**, 082701 (2017).
[53]J. Lindl, O. Landen, J. Edwards, E. Moses, and NIC Team, "Review of the National Ignition Campaign 2009-2012," Phys. Plasmas **21**, 020501 (2014).
[54]M. B. Schneider, S. A. MacLaren, K. Widmann, N. B. Meezan, J. H. Hammer, B. E. Yoxall *et al.*, "The size and structure of the entrance hole in gas-filled hohlraums at the National Ignition Facility," Phys. Plasmas **22**, 122705 (2015).
[55]O. A. Hurricane, D. A. Callahan, D. T. Casey, P. M. Celliers, C. Cerjan, E. L. Dewald *et al.*, "Fuel gain exceeding unity in an inertially confined fusion implosion," Nature **506**, 343 (2014).
[56]F. Wang, S. Jiang, Y. Ding, S. Liu, J. Yang, S. Li *et al.*, "Recent diagnostic developments at the 100 kJ-level laser facility in China," Matter Radiat. Extremes **5**, 035201 (2020).
[57]J. Lindl, "Overview and status of the National Ignition Campaign on the NIF," in Workshop on the Science of Fusion Ignition on NIF, San Ramon, CA, USA, May 22–24, 2012.
[58]L. F. Berzak Hopkins, N. B. Meezan, S. Le Pape, L. Divol, A. J. Mackinnon, D. D. Ho *et al.*, "First high-convergence cryogenic implosion in a near-vacuum hohlraum," Phys. Rev. Lett. **114**, 175001 (2015).
[59]A. L. Kritcher, A. B. Zylstra, D. A. Callahan, O. A. Hurricane *et al.*, "Achieving record hot spot energies with large HDC implosions on NIF in HYBRID-E," Phys. Plasmas **28**, 072706 (2021).
[60]G. Ren, K. Lan, Y.-H. Chen, Y. Li, C. Zhai, and J. Liu, "Octahedral spherical hohlraum for Rev. 6 NIF beryllium capsule," Phys. Plasmas **25**, 102701 (2018).
[61]X. Qiao and K. Lan, "Novel target designs to mitigate hydrodynamic instabilities growth in inertial confinement fusion," Phys. Rev. Lett. **126**, 185001 (2021).